Available online at www.sciencedirect.com
ScienceDirect
Journal of the European Ceramic Society 29 (2009) 1403–1411
www.elsevier.com/locate/jeurceramsoc

Investigation of reactions between vanadium oxide and plasma-sprayed yttria-stabilized zirconia coatings

Zun Chen [a], Scott Speakman [b], Jane Howe [b], Hsin Wang [b], Wally Porter [b], Rodney Trice [a,*]

[a] *Purdue University, West Lafayette, IN 47907-2044, United States*
[b] *Oak Ridge National Laboratory, Oak Ridge, TN 37831-6087, United States*

Received 11 July 2008; received in revised form 28 August 2008; accepted 12 September 2008
Available online 5 November 2008

Abstract

The phase evolution occurring during the reaction between corrosive V_2O_5 ($T_m = 690\,^{\circ}C$) and a plasma-sprayed 7 wt.% Y_2O_3–ZrO_2 (YSZ) coating from 700 to 900 °C has been investigated *in situ* by X-ray diffraction. The temperature and time of interaction between the V_2O_5 and YSZ coating determines the phases observed. Between 700 and 750 °C, reaction products of ZrV_2O_7 and YVO_4 were observed within minutes of reaching the test temperature. m-ZrO_2 was observed after 220 and 60 min at 700 and 750 °C, respectively. The simultaneous formation of both ZrV_2O_7 and YVO_4 at the beginning of the reaction along with the delay of the m-ZrO_2 formation suggests similar reactivity between both Zr and Y with V_2O_5. The weight percent of the ZrV_2O_7 phase began to diminish after 150 and 60 min at 700 and 750 °C, respectively. For reaction temperatures of 800 and 900 °C, there is a rapid decrease in the amount of t′-ZrO_2 and a rapid increase in the amount of m-ZrO_2 with reaction time. YVO_4 was also observed at these reaction temperatures. SEM and TEM microstructural observations confirmed the phases detected from the *in situ* XRD experiments. Reactions between YSZ and V_2O_5 suggest that the formation of a liquid phase due to the high solubility of both zirconia and yttria in vanadia is the dominate mechanism that damages the coating. The thermal conductivity of a plasma-sprayed YSZ coating reacted with up to 1 wt.% V_2O_5 did not significantly change due to the small volume affected.

Keywords: ZrO_2; Corrosion; V_2O_5; Y_2O_3

1. Introduction

Thermal barrier coatings (TBCs) are used in gas turbine engines to protect hot section metallic components from temperature extremes.[1] The thermal protection afforded from the use of a thin ceramic coating, typically 7 wt.% Y_2O_3–ZrO_2 (YSZ), allows higher operating temperatures, with the net effect of improving gas turbine efficiency. However, TBCs are not just subject to temperature extremes during service. With motivation to use less refined fuels due to rising fuel costs comes exposure of the TBC to impurities found in the consumed gas.[2] Severe hot corrosion problem arises when impurities in less-refined fuels, such as Na, S and V, form molten salt/oxide and deposit on the engine surface.[3] Because of the accelerated failure rate of TBCs in hot corrosion environments, durability concerns restrain their use.[4] Of interest in this study is vanadium oxide ($T_m = \sim 690\,^{\circ}C$), a corrosive species that is particular aggressive in its attack of YSZ.[5,6]

In general, chemical interactions between zirconia-based TBCs and a molten oxide degrade the coating, the severity of which increases as the relative acidity to basicity between the two materials increases. The reaction between V_2O_5 and metal oxides like ZrO_2 and common zirconia stabilizers have been proposed to follow a Lewis acid–base mechanism.[7,8] Thus, metal oxides with the strongest basicity (or least acidity) will react most severely with the highly acidic V_2O_5. Since the acidity of Y_2O_3 is low relative to the ZrO_2, it is believed the molten oxide aggressively attacks the stabilizer, while only minimally attacking the more acidic ZrO_2.[7,9]

As is well established, plasma-sprayed YSZ powders form a non-equilibrium tetragonal phase containing 7 wt.% Y_2O_3 (referred to as t′-ZrO_2),[10] whereas the equilibrium composition

* Corresponding author. Tel.: +1 765 494 6405.
E-mail address: rtrice@purdue.edu (R. Trice).

0955-2219/$ – see front matter © 2008 Elsevier Ltd. All rights reserved.
doi:10.1016/j.jeurceramsoc.2008.09.016

for tetragonal zirconia (referred to as t-ZrO_2) would contain ~4 wt.% Y_2O_3.[11] When YSZ coatings composed of t′-ZrO_2 are put in service at representative gas turbine operating temperatures (1100–1200 °C), they begin to partition into equilibrium composition t-ZrO_2 (4 wt.% Y_2O_3) and c-ZrO_2 (14 wt.% Y_2O_3). Partitioning occurs via the migration of the excess Y_2O_3 found in the t′-ZrO_2 to form c-ZrO_2, and this transformation does not occur unless the coating is exposed to 1200 °C for 50+ h.[12,13]

In the presence of molten vanadium compounds the destabilization of the t′-ZrO_2 phase via the formation of YVO_4 and intermediate or equilibrium zirconia phases is much faster than that due to partitioning. The reaction mechanism, however, remains unclear.[14–18] Further complicating the analysis is that Na_2SO_4 is often combined with V_2O_5 to produce the corrosive species, and this combination is less reactive with the coating.[13–16] Published accounts of reactions above ~750 °C describe yttria, which is basic with respect to the acidic V_2O_5, being sequestered or leached from the t′-ZrO_2 by the corrosive agent to form YVO_4.[5–7] According to these reports, removal of the yttria stabilizer from the zirconia leaves unstabilized zirconia (i.e. m-ZrO_2), which is relatively stable with respect to the V_2O_5. Furthermore, reaction of V_2O_5 with c-ZrO_2 above 800 °C suggested that the Y^{3+} in the lattice had the mobility to migrate preferentially toward the reaction interface due to the high V concentration present on the surface.[6]

In this study, the interaction between plasma-sprayed YSZ and V_2O_5 is reexamined via a semi-quantitative *in situ* XRD technique with an emphasis on how the corrosive species attacks both the yttria stabilizer and the zirconia. This approach tracked the sequential crystalline phase evolution at temperatures above the melting temperature of V_2O_5, affording detection of intermediate phases that have been inaccessible when examining the post-reaction phase assemblage. Moreover, microstructural observation of the contaminated coating was incorporated to clarify the interaction mechanism. Finally, the effect of V_2O_5 attack on the thermal conductivity of YSZ has been determined as this property is important in thermal barrier applications.

2. Experimental procedure

2.1. Specimen preparation

A 7 wt.% Y_2O_3–ZrO_2 (YSZ) powder with an average particle size of 22 μm (H.C. Starck, Amperit 825.0) was air-plasma sprayed using a Praxair SG-100 gun at Ames National Laboratory using a gun power of 38 kW, a stand-off distance of 10 cm, and a Ar (25 slm)/He (21 slm) created plasma. The flow rate of the Ar carrying the YSZ powder was 6 slm. Flat copper plate substrates of 102 mm × 76 mm × 5 mm were grit blasted with 24-grit $A1_2O_3$ at 5.5×10^5 Pa prior to being sprayed. The substrates were back-cooled with air jets while sprayed upon from a stand-off distance of ~10 cm. Stand-alone coatings were obtained by dissolving the Cu substrates with nitric acid. The resultant coating thickness varied from 360 to 590 μm. X-ray diffraction experiments at room temperature revealed the coating to be comprised of only t′-ZrO_2 phase. Archimedes experiments[19] in water indicated a total porosity of 10.8% based on a theoretical density of 6.08 g/cm^3. The coatings were subsequently sectioned into 1 cm × 1 cm squares with a diamond-coated saw for corrosion tests.

2.2. Incorporation of V_2O_5 onto the coating

V_2O_5 powder[1] was ball-milled with ethanol and a dispersant[2] for 48 h using zirconia milling media. The V_2O_5 slurry was subsequently applied on the coating surface to an area density of ~0.4 or ~4 mg/cm (corresponding to 0.1% and 1% of the mass of the coating specimen) by air-brushing either dilute or concentrated slurry, respectively. A region 1 mm from each edge of the 1 cm by 1 cm square coating was left uncontaminated via application of a tape mask prior to spraying. This uncontaminated region allowed some spreading of molten V_2O_5 during the high temperature testing without it spilling over the sample edges.

2.3. In situ XRD measurements

In situ XRD was performed at the High Temperature Materials Laboratory (HTML) at Oak Ridge National Laboratory (ORNL). The phase evolution of plasma-sprayed YSZ samples coated with 1 wt.% V_2O_5 and reacted at 700, 750, 800 and 900 °C were studied. The effect of less V_2O_5 (0.1 wt.%) on the phase evolution of YSZ was also studied, but only at 800 and 900 °C. The diffractometer used was a PANalytical X'Pert Pro equipped with an Anton Paar XRK900 reaction chamber. The sample was placed on a Macor pedestal which was then inserted into the furnace, placing the sample in the center of the heating zone, with temperature monitored by a thermocouple. Despite quickly heating the specimens at a rate of ~100 °C/min to the desired temperature, there was evidence that the reaction began during heat-up. X-ray diffraction (XRD) data were collected during isothermal holds in air and data were collected using Cu Kα radiation and a PANalytical X'Celerator solid-state position-sensitive detector.

In situ XRD data for samples tested at 700 and 750 °C was collected for a total of ~500 min; data collected at 800 and 900 °C was collected for ~120 min. Sixty scans, each 130 s in duration, were collected during the first ~120 min of experiments at 700 and 750 °C. A small range of 2θ (23–36°) were collected to avoid missing the initial rapid reaction between V_2O_5 and the YSZ coating. This 2θ range selected afforded detection of primary peaks associated with t′- and m-ZrO_2 phases, as well as the YVO_4 and ZrV_2O_7 phases. All XRD data gathered at 800 and 900 °C was gathered over this narrow 2θ range. After ~120 min XRD scans at 700 and 750 °C were collected at a 2θ range from 15° to 90° over a 1840 s duration. These scans were collected using programmable divergence slits on the incident- and diffracted-beam sides in a variable-slit mode, in which the divergence angle of the slits was varied so that the irradiated length of the sample was constantly 6 mm. For analysis, these

[1] Alfa Aesar (Ward Hill, MA), catalog #11094.
[2] KD-2 from Uniqema, New Castle, DE.

data were corrected so that they corresponded to a fixed 0.5° divergence slit.

XRD data were analyzed using empirical peak fitting and quantitative Rietveld analysis. MDI Jade v6.5[3] was used to empirically fit pseudo-Voigt profile functions to the $\bar{1}11$ and 1 1 1 peaks of m-ZrO_2 phase and to the 1 0 1 peak of t-ZrO_2 phase. Note that the t′-ZrO_2 and t-ZrO_2 1 0 1 peaks overlap, and therefore analysis of the peaks between $2\theta = 72$–76° was used to determine if the 1 0 1 peak was c-ZrO_2, t-ZrO_2 or t′-ZrO_2.[20] No c-ZrO_2 was observed in the as-sprayed or heat-treated coatings based on analysis of the XRD data from 72° to 76°. The integrated peak intensities were then used to determine the fraction of t′-ZrO_2 according to the method of Garvie and Nicholson.[21] Quantitative Rietveld analysis was used to determine the phase fractions of all solid phases in other samples using the program PANalytical HighScore Plus v2.1. Standard crystal structures from the ICSD database were used for m-ZrO_2 (JCPF# 86692), t-ZrO_2 (JCPF# 85322), ZrV_2O_7 (JCPF# 84884), and YVO_4 (JCPF# 2504). The background, specimen displacement, scale factors, lattice parameters, and pseudo-Voigt peak shape factors were typically refined; though some variables, such as lattice parameters and peak shape factors, were held invariant for a phase if it was present in only small quantities (<5 wt.%).

2.4. Thermal conductivity measurements

An Anter FlashLine 5000 thermal diffusivity system (Anter Corporation, Pittsburgh, PA) located at ORNL was used to measure the thermal diffusivity, α, of YSZ coatings with 0, 0.1 wt.% and 1 wt.% V_2O_5 that were heat-treated at 900 °C for 3 h prior to testing. Diffusivity data was acquired every 100 °C from 100 to 1100 °C. Specific heat as a function of temperature of the uncontaminated coating, $c_p(T)$, was measured from 25 to 1200 °C at a heating rate of 20 °C/min using a differential scanning calorimeter (Netzsch Instruments DSC 404C, Burlington, MA). Thermal conductivity, k_{th}, of the coatings was calculated using the following equation,

$$k_{th}(\mathrm{W/m\,K^{-1}}) = \alpha(\mathrm{cm^2/s}) \cdot \rho(\mathrm{g/cm^3}) \cdot c_p(\mathrm{J/g\,K^{-1}}) \cdot 100$$

where ρ is the bulk density and c_p is the specific heat. The as-sprayed coating density used for k_{th} calculations was 5.42 g/cm^3. This density did not change within the experimental detection limits of the Archimedes test after being exposed to temperatures up to 1200 °C.

2.5. Microscopy procedures

To investigate microstructure and vanadium distribution, TEM specimens were made from coatings after they were subject to reaction with V_2O_5 at 750, 800 and 1200 °C. The reaction time at these temperatures varied from 30 to 420 min. Investigation of microstructures at 1200 °C was conducted as this likely represented an equilibrium microstructure. Cross-section TEM specimens were obtained by gluing two pieces of coating together with reacted zones positioned back to back, followed by polishing in the edge-on orientation. A tripod polisher (South Bay Technology) was employed to polish the specimens through a 1 μm diamond paste. The specimen was subsequently mounted on a nickel grid and further thinning was performed in a low-energy Gatan ion mill, model DMP 600. A Hitachi HF-2000 TEM and a JEOL 2010F (S)TEM capable of EDS mapping, located at ORNL and UIUC, respectively, were used for examination. Chemical analysis was performed in the TEM using energy-dispersive X-ray spectroscopy (EDS) point scan and area mapping.

3. Results

3.1. In situ X-ray study of reaction between V_2O_5 and YSZ coating: 700–750 °C

Fig. 1(a) and (b) shows the *in situ* phase assemblage of the t′-ZrO_2 phase in the as-sprayed coating and the reaction products between it and the V_2O_5 as a function of reaction time at 700 and 750 °C, respectively. At the start of the test the predominant phase in the coating was t′-ZrO_2 and liquid V_2O_5 (not detected by XRD). At neither temperature did the t′-ZrO_2 account for 100% of the solid phase at the beginning of the test, suggesting the melted vanadium oxide had already started reacting with the coating upon heating to these temperatures. For this study, zero time is defined upon reaching the reaction temperature and beginning the X-ray scans.

Inspection of Fig. 1(a) reveals simultaneous reactions of V_2O_5 with both zirconia and yttria in the YSZ solid solution. Within the first 2 h of reaction, the amount of t′-ZrO_2 phase decreased dramatically concurrent with the emergence of a ZrV_2O_7 phase (~42 wt.% after 2 h). During the same period, a minor amount of YVO_4 (~2 wt.%) also appeared. It is worth noting that the greater amount of ZrV_2O_7 phase with respect to the YVO_4 phase observed after 2 h is not an indication of the higher reactivity of zirconia with V_2O_5, but rather the greater percentage of ZrV_2O_7 observed is a result of the much higher starting zirconia content (93 wt.%) in YSZ powder than the yttria content (7 wt.%). On the other hand, the results presented in Fig. 1(a) also show that the reaction kinetics between zirconia and V_2O_5 are not slow relative to that between yttria and V_2O_5, as has been previously reported.[7] Following a time period where the wt.% of ZrV_2O_7 is stable (~150–250 min), the wt.% of both the t′-ZrO_2 and ZrV_2O_7 begin to decrease slowly with a concurrent rapid increase in the wt.% of m-ZrO_2.

As shown in Fig. 1(b), the kinetics for formation of ZrV_2O_7 at 750 °C is faster than at 700 °C. The maximum amount of ZrV_2O_7 for the reaction at 750 °C forms after 60 min; the maximum amount of ZrV_2O_7 for the reaction at 700 °C forms after 120 min. At both temperatures, the maximum wt.% of ZrV_2O_7 formed is ~42 wt.%. At 750 °C, the decrease in wt.% of ZrV_2O_7 coincides with an increase in the m-ZrO_2 phases, whereas at 700 °C there appears to be 100 min delay between the peak amount of ZrV_2O_7 and the appearance of the m-ZrO_2 phase. A faster disappearance of the ZrV_2O_7 was observed for the reaction at 750 °C compared to the 700 °C reaction. Furthermore,

[3] Materials Data, Inc. (MDI), Livermore, CA.

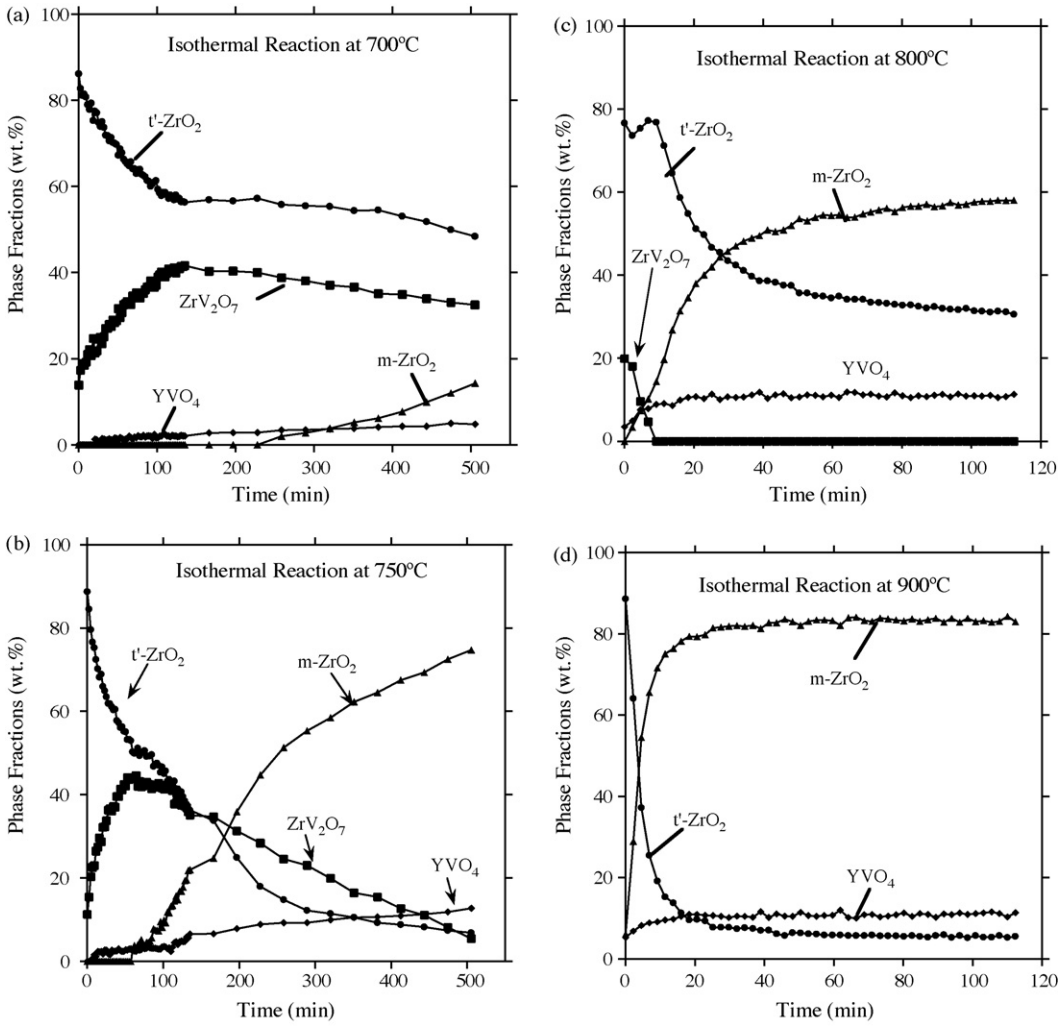

Fig. 1. Diagrams show the phase fraction evolution with time during reactions at isothermal temperatures of (a) 700, (b) 750, (c) 800, and (d) 900 °C. Each sample had 1 wt.% (4 mg/cm^2) V_2O_5 applied to the surface prior to testing. Above 690 °C, the V_2O_5 was melted and therefore not detected by XRD.

there was less ZrV_2O_7 (~10 wt.%) observed after 500 min for reactions at 750 °C than for a similar time at 700 °C (~36 wt.%). At end of 500 min at 750 °C, only 10 wt.% of the t′-ZrO_2 was left compared to 50 wt.% residual t′-ZrO_2 after 500 min at 700 °C. More YVO_4 was also observed (13 wt.%) after reaction at 750 °C than at 700 °C (5 wt.%). Clearly, the 50 °C increase in reaction temperature greatly hastened the corrosion reaction between V_2O_5 and the t'-ZrO_2, not only increasing the rate of ZrV_2O_7 formation, but also its partial decomposition to m-ZrO_2.

It is noted in the XRD data that the amount of the YVO_4 phase continues to increase with time. The source of the vanadium could come from the decomposition of the ZrV_2O_7 phase, from residual vanadium-rich liquid in the system.

3.2. *In situ X-ray study of reaction between V_2O_5 and YSZ coating: 800–900 °C*

Because the phase constituents changed little after ~30 min for each of the experiments at 800 and 900 °C, *in situ* X-ray data was only collected during the first 2 h of reaction. As shown in Fig. 1(c), at 800 °C the intermediate ZrV_2O_7 phase was only observed during the first 10 min of the test. No ZrV_2O_7 was observed for reactions between V_2O_5 and YSZ at 900 °C. YVO_4 is present in both data sets at 800 and 900 °C, respectively. Fig. 1(c) and (d) also shows that the amount of m-ZrO_2 increases from 60 wt.% for the reaction at 800 °C to 83 wt.% for the 900 °C reaction. The amount of residual YVO_4 after 120 min appears to be 2–3 wt.% greater at 900 °C than at 800 °C.

Fig. 2 shows the wt.% of t′-ZrO_2 phase as a function of time at 800 and 900 °C for samples loaded with 0.4 mg/cm^2 V_2O_5 (0.1 wt.% V_2O_5) and 4 mg/cm^2 (1 wt.% V_2O_5). Increasing the amount of corrosive species applied to the surface of the YSZ coating increased the amount of t′-ZrO_2 that transformed to m-ZrO_2 observed at the end of the experiment. This experimental observation is consistent with having more liquid V_2O_5 to dissolve and transform the t′-ZrO_2 into m-ZrO_2 and YVO_4.

3.3. *Microstructural observation of the interaction between V_2O_5 and YSZ*

It is noted in the accompanying paper[22] that two different microstructures develop in V_2O_5 corroded YSZ coatings;

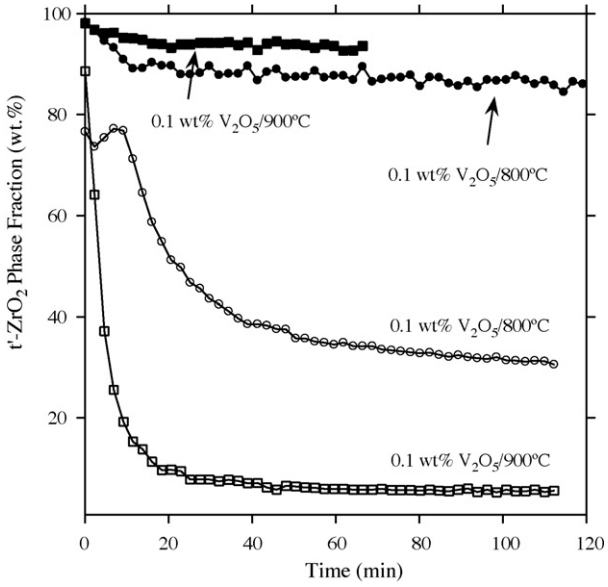

Fig. 2. The wt.% of t′-ZrO_2 as a function of time using data from $2\theta = 23–36°$. Samples with both 1 and 0.1 wt.% V_2O_5 were tested at 800 and 900 °C.

highlights of this paper are provided here. Upon contacting the vanadium-containing melt, the microstructure of the coating undergoes a large-scale change due to a dissolution–precipitation reaction, where the lamellae in the coating are dissolved by the liquid V_2O_5, and precipitate out as clusters of sub-micron equiaxed particles. Near the surface where the V_2O_5 melt is abundant, the transformation of lamellae to particles is complete. This fully reacted region appears as a porous layer of loosely connected or friable particles, which is designated as a planar reaction zone or PRZ[22]. Below the PRZ is a region deemed the melt infiltrated reaction zone or the MIRZ. This region is formed through the infiltration of the coating by the molten V_2O_5 via the interlamellar pores and intralamellar cracks, followed by its reaction with the YSZ. The interaction of V_2O_5 and YSZ with coatings in the MIRZ is essentially the same as in the PRZ, namely through a dissolution–reprecipitation mechanism. The limited supply of V_2O_5 infiltrated through the pores, however, is not sufficient to dissolve the entire lamella; only a thin layer on the surface of the lamella is dissolved instead. The reaction products form scattered fine-particle clusters that are localized in the cracks and/or pores.

3.4. Reaction temperatures of 700–750 °C

Fig. 3 shows STEM micrographs after the coating was reacted with V_2O_5 for 180 min at 750 °C. Based on a EDS spectrum (not shown), a compositional variation was detected in the MIRZ region between the two lamellae shown in Fig. 3(a). A phase containing mostly Zr, V, and O was detected with some signal from Y. This phase is possibly ZrV_2O_7 with some Y detected from the surrounding area. A phase containing Y, V, and O was also detected between the two lamella, indicating the presence of YVO_4. Regions of mostly Zr and O were also detected; these regions were likely m-ZrO_2. Also, the surrounding regions appear to be t′-ZrO_2 based on the presence of Zr, Y, and O. Fig. 3(b) shows an EDS map of a region between two lamella. YVO_4, ZrV_2O_7, and m-ZrO_2 were all observed. Observations of both images in Fig. 3 shows evidence of the reaction products ZrV_2O_7, m-ZrO_2, and YVO_4 co-existing after 180 min reaction at 750 °C, consistent with the *in situ* XRD results presented in Fig. 1(b).

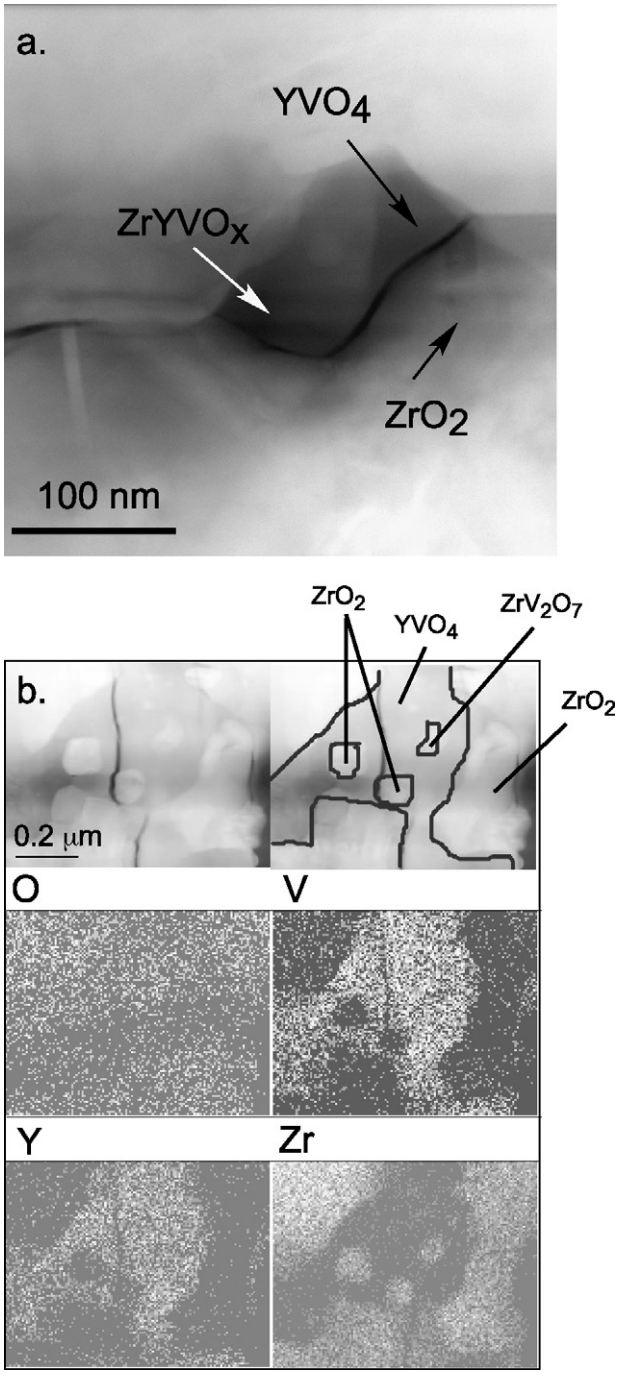

Fig. 3. STEM micrograph in a MIRZ of a coating reacted with V_2O_5 at 750 °C for 180 min. (a) Note the coexistence of YVO_4/ZrV_2O_7 in a particle at lamellar boundary and (b) m-ZrO_2, ZrV_2O_7 and YVO_4, consistent with XRD date presented in Fig. 1(b).

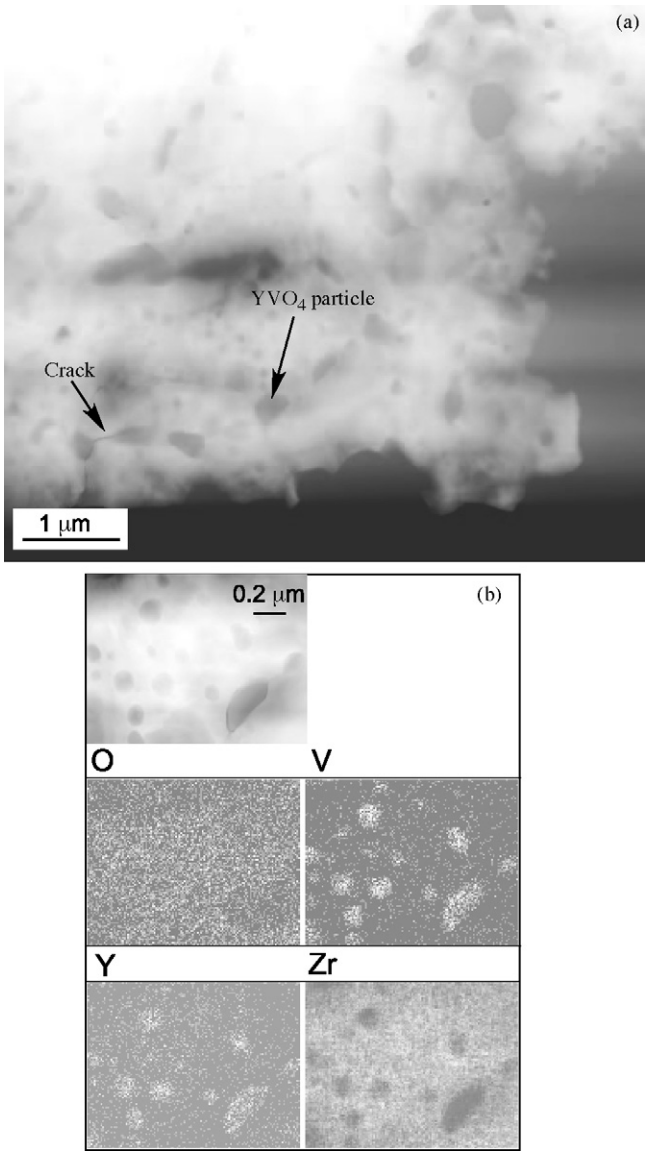

Fig. 4. Cross-sections of PRZ region reacted with 1 wt.% V_2O_5 at 1200 °C for 180 min. (a) A cross-section STEM micrograph shows a slice of the clusters. The contrast in gray scale reflects compositional differences, (b) EDS map shows YVO_4 and m-ZrO_2 in the PRZ region.

3.5. Reaction temperatures of 800–1200 °C

Fig. 4 shows STEM images taken from YSZ samples reacted with 1 wt.% V_2O_5 at 1200 °C for 3 h. The reaction products at 1200 °C were similar to those of samples reacted at 800 and 900 °C; this high reaction temperature was chosen in an effort to observe equilibrium microstructures after short reaction times. Fig. 4(a) shows a PRZ region (near the coating surface) composed of high-contrast grains with a diameter of 50–200 nm imbedded in a gray matrix. EDS mapping of elements Zr, Y, V and O and shows that the high-contrast grains are rich in Y and V (Fig. 4(b)) while the matrix has a negligible amount of Y and V and is composed of primarily Zr and O. Thus, it appears that the nanometer sized grains are YVO_4, while the matrix is m-ZrO_2. STEM images taken from m-ZrO_2 regions (not shown)

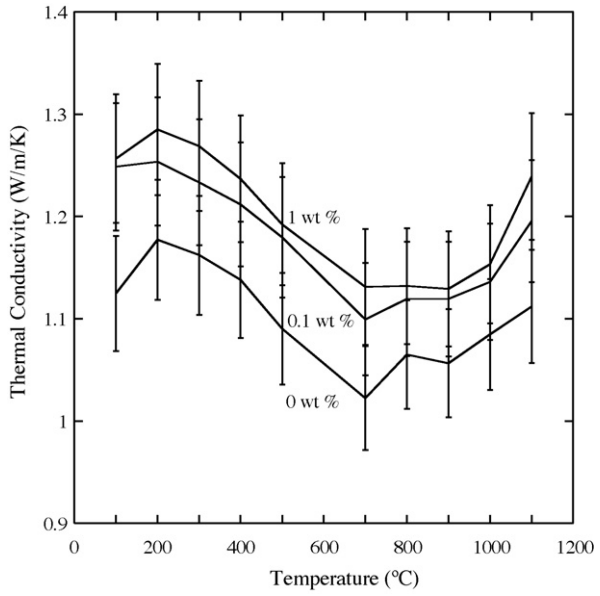

Fig. 5. The thermal conductivity of YSZ coatings after reacting with 0, 0.1 wt.% and 1 wt.% V_2O_5 for 3 h at 900 °C is plotted against measurment temperature. The corresponding V_2O_5 loading is indicated beside the curve. Errors of ±6% of the measured values were estimated.

indicated a twinned structure common in monoclinic zirconia. EDS results from these grains indicated no Y and negligible V concentrations. It is clear that the as-sprayed t′-ZrO_2 has now transformed into m-ZrO_2 and YVO_4 mixed on a very small scale, consistent with *in situ* XRD results presented in Fig. 1(c) and (d). Microstructure investigation did not verify the presence of ZrV_2O_7 above 800 °C, consistent with *in situ* XRD results.

3.6. Thermal conductivity measurements

Thermal diffusivity measurements from 100 through 1100 °C were made on coatings previously reacted for 3-h, at 900 °C with 0, 0.1 and 1 wt.% V_2O_5. As stated in the experimental procedure, thermal diffusivity values at each temperature measured were multiplied by density and specific heat to generate thermal conductivity values. Fig. 5 presents these results. In general, a decrease in k_{th} was observed from 100 through 700 °C due to increased lattice vibrations, followed by an increase in k_{th} through 1100 °C due to sintering. The uncontaminated coating demonstrated the lowest thermal conductivity, and the 1 wt.% V_2O_5 contaminated coating showed slightly higher thermal conductivity than the 0.1 wt.% contaminated coating. As m-ZrO_2, the predominant phase observed after reaction of V_2O_5 with YSZ at 900 °C (see Fig. 1(d)), has a higher thermal conductivity than t′-ZrO_2 this trend would be expected.[23] However, based on 6% error associated with these measurements, difference in thermal conductivity is not likely of statistical significance. In addition, thermal conductivity measured *in situ* during reaction with 1 wt.% V_2O_5 at 900 °C (results not shown here) also showed no statistical difference from that of the uncontaminated coatings. Thus, the thermal properties of YSZ are not significantly affected by the reaction with up to 1 wt.% V_2O_5 because the thickness of the PRZ and MIRZ combined is nor-

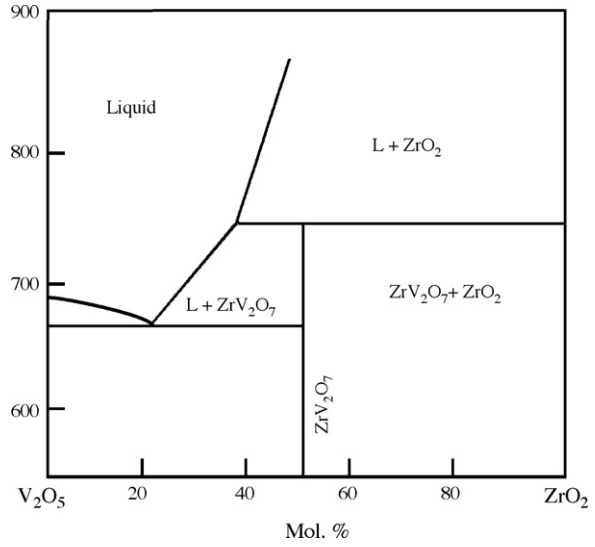

Fig. 6. ZrO_2–V_2O_5 binary phase diagram. Adapted from Ref.[24]

mally 50–60 μm, which accounts for only a small proportion of the total coating thickness of ~300 μm.

4. Discussion

The reactions between V_2O_5 and zirconia at 700 and 750 °C are consistent with the ZrO_2–V_2O_5 phase diagram[24] shown in Fig. 6. Beginning with pure V_2O_5 in contact with the YSZ at 700 °C, the liquid V_2O_5 can dissolve approximately 30 mol.% zirconia in solution before the first solid reaction product (ZrV_2O_7) will form. For compositions of 50 mol.% V_2O_5/50 mol.% ZrO_2, only ZrV_2O_7 should be present. If the V_2O_5 concentration continues to decrease beyond 50 mol.%, m-ZrO_2 should precipitate out of the ZrV_2O_7 phase. According to the Y_2O_3–V_2O_5 phase diagram[24] (not shown), above 690 °C liquid V_2O_5 will dissolve significant amounts of Y_2O_3. For example, at 750 and 900 °C vanadium oxide can dissolve up to ~5 and ~10 mol.% Y_2O_3, respectively. Beyond these temperature-dependent saturation limits, YVO_4 precipitates out of the liquid. Thus, based on consideration of the phase diagrams, it would be expected that V_2O_5 would dissolve both ZrO_2 and Y_2O_3 solid phases at temperatures above 690 °C. At or below 750 °C, ZrV_2O_7 should be the first reaction product formed from the reaction of ZrO_2 and V_2O_5, followed by precipitation of m-ZO_2 as the vanadium oxide concentration continues to diminish. YVO_4 is the reaction product between Y_2O_3 and V_2O_5 for all temperatures considered currently. This interpretation of the phase diagrams is consistent with the XRD data in Fig. 1(a) and (b) as both the formation of ZrV_2O_7 and YVO_4 occurred simultaneously, with the formation of m-ZrO_2 occurring later.

From the phase diagram presented in Fig. 6, ZrV_2O_7 would not be expected for reaction temperatures of 800 and 900 °C as its formation is above the peritectic reaction (L + m-ZrO_2 → ZrV_2O_7) occurring at ~750 °C. However, as noted in Fig. 1(c), a limited amount of ZrV_2O_7 was noted through the first 10 min of the test at 800 °C. It is believed that its formation occurs during transient heating of the V_2O_5-coated YSZ sample through temperatures lower than 750 °C. Fig. 1(d) shows that at 900 °C no ZrV_2O_7 was observed. The phase diagram for V_2O_5 and ZrO_2 (see Fig. 6) above the peritectic temperature indicates that liquid V_2O_5 can dissolve ~40 and ~50 mol.% ZrO_2 at 800 and 900 °C, respectively. m-ZrO_2 should form beyond these temperature-dependent saturation limits, consistent with XRD data in Fig. 1(c) and (d).

As stated previously, published accounts[7,9] describe zirconia as having good resistance to vanadium oxide hot corrosion in that it reacts slowly with V_2O_5. This is certainly not the case for reaction temperatures below 750 °C, where the V_2O_5 and the YSZ coating react to form ZrV_2O_7 within minutes of reaching 700 °C (see Fig. 1(a) and (b)). Concomitant with the formation of ZrV_2O_7 is the formation of YVO_4, suggesting similar reactivity between m-ZrO_2 and V_2O_5, and Y_2O_3 and V_2O_5. Fig. 3(a) and (b) confirmed the presence of both YVO_4 and ZrV_2O_7 in a YSZ coating reacted for 180 min at 750 °C, corroborating the XRD results. It is interesting to note that if V_2O_5 reacted preferentially with yttrium rather than the zirconium, the areas of the coating that were depleted of its stabilizer would have formed m-ZrO_2 concurrently with the formation of the YVO_4. However, results in Fig. 1a show that no m-ZrO_2 was observed during the initial 220 min of the experiment at 700 °C. The incubation period before the appearance of m-ZrO_2 suggests that the t′-ZrO_2 phase was not depleted of Y_2O_5 to such an extent that the t → m transformation would begin. Therefore, the following concurrent reactions have fairly similar reaction rates at 700 °C and 750 °C, resulting in a dramatic decrease of the t′-ZrO_2:

$$ZrO_2\,(\text{in t}'\text{-}ZrO_2) + V_2O_{5(\text{liquid})} \rightarrow ZrV_2O_7 \quad (1)$$

$$Y_2O_3(\text{in t}'\text{-}ZrO_2) + V_2O_{5(\text{liquid})} \rightarrow YVO_4 \quad (2)$$

Thus, both yttrium and zirconium demonstrate similar susceptibility to corrosion by vanadium oxide below 750 °C.

According to the ZrO_2–V_2O_5 phase diagram (Fig. 6), above 750 °C m-ZrO_2 does appear to be unreactive with respect to the V_2O_5 in the sense that a new compound is not formed. But, this does not imply the zirconia-based coating is unaffected by the molten liquid as at all temperatures above 690 °C zirconia has significant solubility in the melted V_2O_5 (see Fig. 6). Thus, the coating will be locally dissolved by the correndent. As the composition of the liquid phase containing V, Y, Zr, and O changes, solid phases of YVO_4 and m-ZrO_2 are precipitated. This dissolution/precipitation reaction gives rise to the equiaxed microstructure observed in the planar reaction zone, and within the pores and cracks of the melt infiltrated reaction zone. Thus, the microstructures formed are consistent with the formation of liquid, and precipitation of solid phases from that liquid.

Hertl[6] has noted that the yttria used as a stabilizer is sequestered or leached from the YSZ by the V_2O_5 to form YVO_4 due to its high mobility, leaving behind unstabilized zirconia or m-ZrO_2. This seems unlikely as the t′-ZrO_2 partitioning reaction, which is controlled by the diffusion of Y atoms, is slow at temperatures as high as 1200 °C. It is more likely that the kinetics of YVO_4 development at 800 and 900 °C are dominated by the formation of the eutectic liquid between V_2O_5, ZrO_2, and

Y_2O_3, which would afford rapid diffusion of Y. As shown in the companion paper, the microstructure of the reacted coating nearest the surface (where the V_2O_5 is applied) appears as equiaxed grains rather than the lamella microstructure expected for plasma-sprayed coatings. If leaching of yttria was the primary reaction, residual lamella structure would be expected to be observed rather than the equiaxed particles noted in the PRZ.

The implication of the current work is that zirconia-based ceramics have very limited resistance to V_2O_5 because of the susceptibility of ZrO_2 to be dissolved by this species, regardless of whether or not a new crystalline by product immediately results. Furthermore, the nature of the zirconia-stabilizer would not limit the reaction of the V_2O_5 with the coating because of the high solubility of the majority phase, i.e. the zironia. Thus, a more acidic stabilizer than yttria would not be able to prevent the catastrophic degradation of zirconia in V_2O_5 simply because of its solubility in vanadium oxide. Therefore, a search for zirconia stabilizers less basic than Y_2O_3, like In_2O_3, Sc_2O_3, or CeO_2,[7,25–27] with the goal to design a thermal barrier more corrosion-resistant than Y_2O_3-stabilized ZrO_2, is not likely to be successful.

5. Summary

In situ XRD experiments investigating the reaction products between V_2O_5 and YSZ at temperatures ranging from 700 through 900 °C were conducted. Reaction products of ZrV_2O_7, m-ZrO_2 and YVO_4 were observed, with ZrV_2O_7 only observed for experiments at 700 and 750 °C. Concurrent formation of ZrV_2O_7 and YVO_4 at 700 and 750 °C suggests a similar reactivity of yttrium and zirconia with vanadium oxide. The ZrV_2O_7 phase, however, was not stable; *in situ* X-ray diffraction revealed its subsequent partial decomposition after 150 and 60 min at 700 and 750 °C, respectively. While m-ZrO_2 is stable with respect to V_2O_5 for reaction temperatures above 750 °C in that interactions between these two compounds do not form a new compound, zirconia is not unaffected by the molten liquid due to its high solubility in the vanadia. Thus, lamellae in the YSZ coating in contact with vanadium oxide melt are completely dissolved by the corrosive liquid. YVO_4 and m-ZrO_2 are both precipitated from the melt, forming the equiaxed composite particles found in the PRZ layer of the coating. With up to 1 wt.% of V_2O_5, thermal conductivity of the coating was not significantly affected.

Acknowledgements

This work was supported by Purdue Research Foundation and by the National Science Foundation through DMR-0134286. Research sponsored by the Assistant Secretary for Energy Efficiency and Renewable Energy, Office of FreedomCAR and Vehicle Technologies, as part of the High Temperature Materials Laboratory User Program, Oak Ridge National Laboratory, managed by UT-Batelle, LLC, for the U.S. Department of Energy under contract number DE-AC05-00OR22725.

References

1. Miller, R. A., Current status of thermal barrier coatings—an overview. *Surf. Coat. Technol.*, 1987, **30**, 1–11.
2. Trembly, J. P., Gemmen, R. S. and Bayless, D. J., The effect of IGFC warm gas cleanup system conditions on the gas–solid partitioning and form of trace species in coal syngas and their interactions with SOFC anodes. *J. Power Sources*, 2007, **163**(2), 986–996.
3. Miller, R. A., Ceramic thermal barrier coatings for electric utility gas turbine engines. NASA TM-87288, 1986.
4. Jones, R. L., Some aspects of the hot corrosion of thermal barrier coatings. *J. Therm. Spray Technol.*, 1997, **6**(1), 77–84.
5. Susnitzky, D. W., Hertl, W. and Carter, C. B., Destabilization of zirconia thermal barriers in the presence of V_2O_5. *J. Am. Ceram. Soc.*, 1988, **71**(11), 992–1004.
6. Hertl, W., Vanadia reaction with yttria stabilized zirconia. *J. Appl. Phys.*, 1988, **63**(11), 5514–5520.
7. Jones, R. L., Williams, C. and Jones, S., Reaction of vanadium compounds with ceramic oxides. *J. Electrochem. Soc: Solid-State Sci. Technol.*, 1986, **133**(1), 227–230.
8. Belykh, D. B., Zhabrev, V. A., Zaitsev, S. V., Glushkova, V. B. and Krzhizhanovskaya, V. A., Interaction of Y_2O_3-stabilized cubic ZrO_2 with sodium silicate and sodium aluminosilicate glass-forming melts. *Glass Phys. Chem.*, 2002, **28**(1), 36–39.
9. Jones, R. L. and Williams, C. E., Hot corrosion studies of zirconia ceramics. *Surf. Coat. Technol.*, 1987, **32**, 349–358.
10. Lelait, L., Alperine, S., Diot, C. and Mevrel, M., Thermal barrier coatings: microstructural investigation after annealing. *Mater. Sci. Eng. A*, 1989, **121**, 475–482.
11. Stevens, R., *Introduction to Zirconia*. Magnesium Elektron Publication, 1986, p. 113.
12. Lelait, L., Alperine, S., Diot, C. and Mevrel, M., Thermal barrier coatings—microstructural investigation after annealing. *Mater. Sci. Eng. A*, 1989, **120**, 475–482.
13. Trice, R. W., Su, Y. J., Mawdsley, J. R., Faber, K. T., De Arellano-Lopez, A. R., Wang, H. *et al.*, Effect of heat-treatment on phase stability, microstructure, and thermal conductivity of plasma-sprayed YSZ. *J. Mater. Sci.*, 2002, **37**, 2359–2365.
14. Gurrappa, I., Thermal barrier coatings for hot corrosion resistance of CM 247 LC superalloy. *J. Mater. Sci. Lett.*, 1998, **17**, 1267–1269.
15. Tsai, P. and Hsu, C., High temperature corrosion resistance and microstructural evolution of laser-glazed plasma-sprayed zirconia/MCrAlY thermal barrier coatings. *Surf. Coat. Technol.*, 2004, **183**(1), 29–34.
16. Marple, B. R., Voyer, J., Moreau, C. and Nagy, D. R., Corrosion of thermal barrier coating by vanadium and sulfur compounds. *Mater. High Temp.*, 2000, **17**(3), 397–412.
17. Mifune, N., Harada, Y., Doj, T. and Yamasaki, R., Hot-corrosion behavior of graded thermal barrier coatings formed by plasma-spraying process. *J. Therm. Spray Technol.*, 2004, **13**(4), 561–569.
18. Mohan, P., Yuan, B., Patterson, T., Desai, V. and Sohn, Y., Degradation of yttria-stabilized zirconia thermal barrier coatings by vanadium pentoxide, phosphorous pentoxide, and sodium sulfate. *J. Am. Ceram. Soc.*, 2007, **90**(11), 3601–3607.
19. ASTM C373-77, Standard Test Method for water absorption bulk density, apparent porosity and apparent specific gravity of fired whiteware products. 1997.
20. Muraleedharan, K., Subrahmanyam, J. and Bhaduri, S. B., Identification of T' phase in ZrO_2–7.5 wt.% Y_2O_3 thermal barrier coatings. *J. Am. Ceram. Soc.*, 1988, **71**(5), C226–C227.
21. Garvie, R. and Nicholson, P., Phase analysis in zirconia systems. *J. Am. Ceram. Soc.*, 1972, **55**(6), 303–305.
22. Chen, Z., Mabon, J., Wen, J.-G. and Trice, R.W., Degradation of plasma-sprayed yttria-stabilized zirconia coatings via ingress of vanadium oxide. *J. Eur. Ceram. Soc.*, doi:10.1016/j.jeurceramsoc.2008.10.003, in press.
23. Hasselman, D. P. H., Johnson, L. F., Bentsen, L. D., Syed, R., Lee, H. L. and Swain, M. V., Thermal diffusivity and conductivity of dense polycrystalline ZrO_2 ceramics: a survey. *Am. Ceram. Soc. Bull.*, 1987, **66**(5), 799–806.

24. Reser, M. K., ed., *Phase Diagrams for Ceramists–1969*. The American Ceramic Society, Columbus, OH, 1969, Supplement, Fig. 2405.
25. Jones, R. L., Scadia-stabilized zirconia for resistance to molten vanadate-sulfate corrosion. *Surf. Coat. Technol.*, 1989, **39/40**, 89–96.
26. Jones, R. L., Reidy, R. F. and Mess, D., Scandia, yttria-stabilized zirconia for thermal barrier coatings. *Surf. Coat. Technol.*, 1996, **82**, 70–76.
27. Jones, R. L. and Mess, E., India as a hot corrosion-resistant stabilizer for zirconia. *J. Am. Ceram. Soc.*, 1992, **75**(7), 1818–1821.